Research Article Vol. 33, No. 5 / 10 Mar 2025 / Optics Express 9117
Optics EXPRESS

Multi-grid parallel ptychographic algorithm for frequency-resolved optical gating

FUCAI DING,[1,2] PING ZHU,[1,4] RANA JAFARI,[3] ZEZHAO GONG,[1,2] YOUJIAN YI,[1,2] XUEJIE ZHANG,[1] DONGJUN ZHANG,[1] XIAOPING OUYANG,[1] XINGLONG XIE,[1] JIANQIANG ZHU,[1,5] AND RICK TREBINO[3,6]

[1]*Key Laboratory of High Power Laser and Physics, Shanghai Institute of Optics and Fine Mechanics, Chinese Academy of Sciences, Shanghai 201800, China*
[2]*Center of Materials Science and Optoelectronics Engineering, University of Chinese Academy of Sciences, Beijing 100049, China*
[3]*School of Physics, Georgia Institute of Technology, 837 State Street, Atlanta, Georgia 30332, USA*
[4]*zhp1990@siom.ac.cn*
[5]*jqzhu@siom.ac.cn*
[6]*rick.trebino@physics.gatech.edu*

Abstract: The ptychographic reconstruction algorithm is a commonly utilized method for pulse phase retrieval due to its super-resolution and robustness, allowing it to retrieve pulses from incomplete traces. However, the algorithm's performance can be hindered by occasional convergence stagnation caused by local minima in the gradient descent strategy. To address this issue, we propose a pulse reconstruction approach for frequency-resolved optical gating (FROG), which employs a multi-grid flexible sampling and parallel extended ptychographic iterative engine (ePIE), ultimately converging to the global FROG trace. The approach can effectively escape from the local minima and demonstrates extremely stable convergence without any prior information. We demonstrate, numerically and experimentally, that this approach can converge well to the correct pulse, especially for complex pulse reconstruction, even in cases of high noise and highly incomplete traces.

1. Introduction

The role of the amplitude and phase characteristics of ultrashort pulses is crucial in high-power laser devices and laser–matter interactions. However, measuring these pulses presents several practical challenges, including the need for high time/spectral resolution, stability, and noise robustness. Various characterization techniques and their corresponding pulse retrieval algorithms have been developed. Spectral phase interferometry for direct electric field reconstruction (SPIDER) utilizes chirped pulses and sum-frequency generation to achieve spectral shear. The pulses are subsequently reconstructed using direct, non-iterative algorithms [1,2]. Self-referenced spectral interferometry (SRSI) necessitates only a minimal number of iterations for pulse reconstruction, yet the measurable pulse width is constrained [3]. Dispersion scan (D-scan) has been recently developed for the measurement of few-cycle pulses [4]. The pulse can then be reconstructed using multidimensional optimization algorithms [5]. Frequency-resolved optical gating (FROG) is the first technique that can completely characterize ultrafast laser pulses without assumptions required by group velocity measurement [6–8]. It utilizes a reference pulse and a measurement pulse to generate second-order or higher-order nonlinear phenomena. The delay-frequency image of the output signal, known as the FROG trace, is then measured, enabling an indirect measurement of the pulses. This method leverages data diversity to convert the unsolvable one-dimensional phase recovery problem into a solvable two-dimensional phase recovery problem. The unique solution of the FROG measurement has been theoretically validated, barring certain trivial ambiguities

#543471 https://doi.org/10.1364/OE.543471
Journal © 2025 Received 30 Sep 2024; revised 5 Feb 2025; accepted 11 Feb 2025; published 24 Feb 2025

Optics EXPRESS

[7,9]. Indeed, the entire trace, well known to contain massively redundant information (which can in some cases be used to obtain pulse spatiotemporal information), is not required to retrieve the pulse if it is free of spatiotemporal distortions. FROG has matured into a reliable and practical measurement technique. The primary challenge associated with FROG is to find an efficient phase retrieval algorithm.

The most commonly used algorithm for estimating a pulse from its FROG traces is the generalized-projections algorithm [10]. A recent algorithm, known as the Retrieved-Amplitude N-grid Algorithmic (RANA) [11], derives more precise initial estimates from FROG traces by leveraging the Paley–Wiener Theorem and the expected continuity of the signal. Then it combines with the "multi-grid" strategy that facilitates the parallel enhancement of a set of initial estimates derived from smaller FROG traces. Compared to standard generalized-projections algorithm, RANA not only achieves 100% convergence but also significantly accelerates the process for complex pulses, demonstrating exceptional robustness [12]. However, both of these approaches have only been demonstrated for retrieving pulses when all delay steps of the FROG trace have been obtained. The discrete Fourier-transform relation between the time delay and spectral increments and ranges algorithmically imposes couplings between experimental spectral resolution, delay range, delay step, and spectral range. These couplings can potentially complicate the implementation of FROG in certain cases. For instance, it is imperative to ensure that the phase-matching bandwidth of the nonlinear crystal is sufficiently large and exhibits a flat spectral response to prevent trace filtering. Additionally, the reconstruction of a complex pulse with the time-bandwidth product (*TBP*) exceeding 50 necessitates a time-frequency grid of at least 2048×2048 or even larger. This requirement imposes significant challenges on both experimental operations and computational demands.

An algorithm, known as the ptychographic reconstruction algorithm, has been developed to eliminate these restrictions, and is now one of the standard reconstruction algorithms for FROG [13,14]. It is based on ptychography [15], a widely used coherent diffractive imaging (CDI) technology. The extended ptychographical iterative engine (ePIE) is a robust iterative algorithm commonly employed in ptychography [16]. Compared with traditional phase-retrieval algorithms, ePIE does not require prior information on the object and probe beam. Unlike generalized projects, which requires the complete global trace, the ptychographic-based algorithm for FROG can iteratively process the signal spectrum with only partial sets of delays. Consequently, the FROG trace does not need to adhere to the discrete Fourier-transform relations, and the temporal resolution is primarily constrained only by the spectral range. This characteristic of ptychography allows for the reconstruction of a pulse from incomplete FROG traces, which are comprised of a small number of delays or spectral measurements. This approach circumvents the issue of excessively large traces that can make experimental measurement and pulse reconstruction laborious and computationally demanding. Furthermore, it addresses the problem of bandwidth limitations imposed by thick nonlinear crystals. These advantages have broadened the applications of the ptychographic-based algorithm, enabling it to successfully reconstruct few-cycle pulses [17], supercontinuum [18], femtosecond extreme ultra-violet pulses [19,20], and attosecond pulses (FROG-CRAB) [21] from incomplete traces. Moreover, the ptychographic algorithm has been successfully used for reconstruction of an ultrashort laser pulse from flexibly shaped FROG traces [22]. Each of these applications has demonstrated excellent performance. The ptychographic-based algorithm employs a steepest descent strategy to update the estimated pulse, utilizing a single time shift of the FROG trace in each iteration. However, non-smooth and non-convex functions can potentially increase the complexity of convergence, occasionally leading to convergence at local minima and causing stagnation. The probability of encountering incomplete FROG traces, especially when reconstructing complex pulses, is significantly heightened, which may necessitate an increased number of measurements (sample complexity) to recover the

Optics EXPRESS

pulse [23–25]. Furthermore, convergence heavily depends on the update coefficients and prior information, such as measured spectrum [13,26].

In this work, we have effectively addressed these challenges by employing a multi-grid parallel sampling and processing scheme, which is based on the ePIE. This approach decomposes the FROG trace into various sub-traces via two-step direct sampling, thereby facilitating the rapid elimination of inaccurate minima through parallel iterative processes. It enables stable and accurate convergence without any prior information on highly incomplete FROG traces, such as spectrally filtered and temporally down-sampled traces, even in instances with strong noise. Furthermore, the retrieval of extremely complex pulses necessitates only a few delays, significantly reducing the computational load. Simulated and experimental phase retrievals of incomplete traces are shown to demonstrate the stable convergence and robustness of this approach. We refer to this algorithm as the multi-grid parallel ptychographic algorithm (MPPA).

2. Method

2.1. Multi-grid parallel ptychographic algorithm

The main idea of the MPPA is to concurrently and expeditiously process the multi-scale sub-datasets in parallel prior to full-resolution FROG analysis, thereby achieving correction and screening of initial guesses, significantly improving the convergence of ultrashort pulse reconstruction. The algorithm leverages the overdetermined nature of pulse characterization via FROG measurements. It has been mathematically proven that, in the absence of prior information, a FROG trace comprising only three delays can validate a pulse [27]. The FROG trace with M spectral components and N delay steps can be sampled into smaller sub-traces based on the multi-grid method and process them separately and parallelly [28]. The MPPA employs parallel ePIE to perform time-domain phase retrieval through hierarchical processing of subsampled FROG traces [29,30]. Figure 1(a) presents the schematic diagram of the MPPA, encompassing multi-grid flexible sampling, parallel-ePIE reconstruction, and final electric field reconstruction.

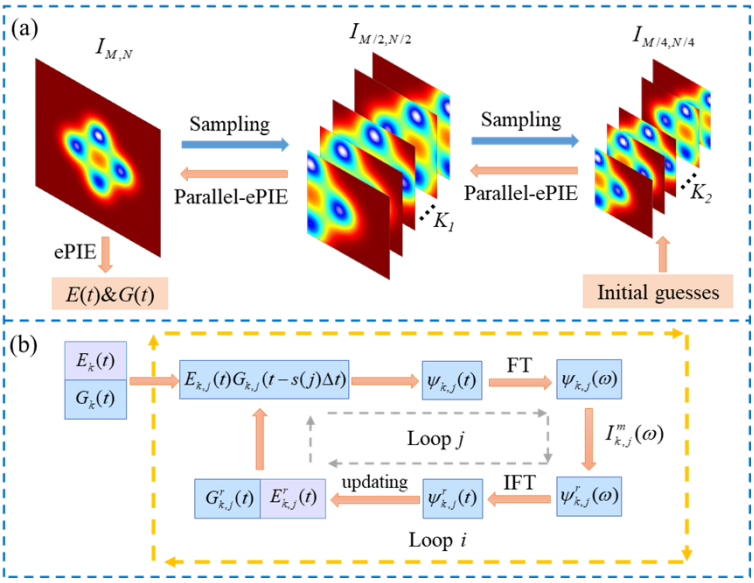

Fig. 1. (a) Schematic diagram of MPPA. (b) Parallel-ePIE iteration flow chart.

Optics EXPRESS

First, the MPPA implements a two-stage direct sampling scheme without strict adherence to the discrete Fourier relationship between delay (τ) and frequency (ω) axes. The sampling steps are defined as follows:

1. $I_{M/2,\,N/2}$ sub-traces: Extract K_1 sub-traces by windowing the central region of $I_{M,\,N}$:

$$I^{k_1}_{M/2,N/2} = \mathbf{C}\{I_{M,N}(\frac{M}{4}+1:\frac{3M}{4},\frac{N}{4}+1:\frac{3N}{4})\}, \tag{1}$$

   where $k_1 = 1, 2, \cdots, K_1$, $\mathbf{C}$ represents the central cropping operator, and scanning along the delay axis generates K_1 sub-traces. This process preserves the core spectral features of the original signal.

2. $I_{M/4,\,N/4}$ sub-traces: Generate $K_2 = 2K_1$ sub-traces via stride-2 decimation of each $M/2 \times N/2$ trace:

$$I^{k_2}_{M/4,N/4} = I^{k_1}_{M/2,N/2}(2m-\beta, 2n-\beta), \beta \in \{0,1\} \tag{2}$$

   for $m = 1, 2, \cdots, M/4$, $n = 1, 2, \cdots, N/4$.

The reconstruction hierarchy follows an inverse multi-grid scheme that starts with the $M/4 \times N/4$ sub-traces, followed by $M/2 \times N/2$ sub-traces. The random initial guess of each sub-trace is refined, and poorly performing pulses are eliminated, leaving only the best performing pulses as input to subsequent layer traces. The two-step direct sampling can be executed with relative simplicity, necessitating only the avoidance of excessive spectral truncation to prevent inadequate temporal resolution. In this method, different sub-traces effectively consider almost all the pertinent information of the original trace, thereby enhancing the final convergence and robustness, especially for an incomplete trace.

Then, pulse reconstructions of the sub-traces are performed utilizing parallel ePIE iterations. Figure 1(b) delineates the detailed steps of the parallel-ePIE iteration for the multi-scale sub-traces. The mathematical representation of FROG trace in frequency domains for each scanning delay is:

$$I_j(\omega) = |\mathrm{FT}(\psi_j(t))|^2, \tag{3}$$

where $\psi_j(t) = E(t)G(t - j\Delta\tau)$, $j = 1, 2, \cdots, J$ is the scanning delays index, $\Delta\tau$ is the delay step. FT stands for the Fourier transform operator. $E(t)$ is the complex envelope of the measured pulse (the probe pulse), $G(t)$ is the complex envelope of the gate pulse. Note that for the self-referenced FROG, specifically, for second-harmonic generation (SHG) FROG, $G(t) = E(t)$ and for polarization gating (PG) FROG, $G(t) = |E(t)|^2$.

In Fig. 1(b), $E_k(t)$ and $G_k(t)$ are the initial guesses of the sub-probe pulse and sub-gate pulse, respectively. The initial guesses all just have Gaussian intensity profiles and random phases without any prior information. First, for the internal loop of each delay, multiplying them yields the nonlinear signal of the field:

$$\psi_{k,j}(t) = E_{k,j}(t)G_{k,j}(t - s(j)\Delta\tau), \tag{4}$$

where $k = 1, 2, \cdots, K_1$ *or* K_2, and s is a random array of the integers ranging from 1 to J. Second, the signal is Fourier transformed:

$$\psi_{k,j}(\omega) = \mathrm{FT}[\psi_{j,k}(t)]. \tag{5}$$

Third, the amplitude of $\psi_{k,j}(\omega)$ will be replaced by the square root of the measured spectra after sampling $I^m_{k,j}(\omega)$ at the $s(j)$-th delay. Here we only replace the part that was measured reliably.

Optics EXPRESS

Then the updated signal is calculated by

$$\psi^r_{k,j}(t) = \mathrm{IFT}\left[\frac{\sqrt{I^m_{k,j}(\omega)}}{|\psi_{k,j}(\omega)|}\psi_{k,j}(\omega)\right]. \tag{6}$$

Finally, update the sub-probe pulse and sub-gate pulse according to the following:

$$E^r_{k,j}(t) = E_{k,j}(t) + \alpha_{k,j}\frac{(G_{k,j}(t - s(j)\Delta\tau))*}{|G_{k,j}(t - s(j)\Delta\tau)|^2_{\max}}(\psi^r_{k,j}(t) - \psi_{k,j}(t)), \tag{7}$$

$$G^r_{k,j}(t - s(j)\Delta\tau) = G_{k,j}(t - s(j)\Delta\tau) + \alpha_{k,j}\frac{(E_{k,j}(t))*}{|E_{k,j}(t)|^2_{\max}}(\psi^r_{k,j}(t) - \psi_{k,j}(t)), \tag{8}$$

where the asterisk denotes the complex conjugate operation, $\alpha_{k,j}$ is the update coefficient, which ranges from 0 to 1, can influence both the convergence speed and robustness of the pulse retrieval algorithm. The above steps will be repeated until all the delays have been accounted for, marking the completion of one full iteration cycle within an internal loop. The reconstruction process will terminate after reaching a predetermined number of external loop iterations or the maximum acceptable errors.

The entire reconstruction process is comprised of the parallel and independent reconstruction processes of $M/4 \times N/4$ sub-traces and $M/2 \times N/2$ sub-traces. The MPPA prioritizes pulse reconstruction from low-resolution FROG traces. Subsequently, the pulses with the smallest errors are then interpolated to higher resolutions as the initial guesses for the subsequent grid. Although interpolation introduces errors, these errors will be corrected after several iterations. The parallel-ePIE reconstructions provide a rapid correction and picking for the initial guesses.

Ultimately, these picked pulses serve as the initial guesses, enabling accurate convergence in just a few iterations for the global FROG trace.

2.2. Parallel iteration parameters

The MPPA is capable of extracting a pulse from its notably incomplete FROG trace, despite the presence of significant noise. Importantly, the difficulty of retrieving a pulse from its FROG trace varies significantly, depending on the degree of incompleteness and noise present. Consequently, we propose a weight factor, W, which accounts for both the incompleteness and noise of the trace. The definition of W is as follows:

$$W = (1 - 10^{-\frac{\sigma_{SNR}}{10}\cdot\varepsilon})\eta, \tag{9}$$

where $(1 - 10^{-\frac{\sigma_{SNR}}{10}\cdot\varepsilon})$ is the noise term, σ_{SNR} is the signal-to-noise ratio of the intensity of trace in dB. We utilize an incomplete-trace parameter η, defined as the number of pixels in the incomplete trace divided by the number of pixels of the complete trace, and the incomplete trace represents the information of the reliable and effective part. The frequency and delay axes of the complete trace satisfy the discrete-Fourier relationship, that is, the measured FROG trace consists of $M \times N$ (where $M = N$) points, and the product of delay step and spectral resolution should be $1/N$ [31]. ε is the scaling constant that correlates with the size of the trace or the *TBP* of the pulse. For instance, when the *TBP* is approximately 5, an appropriate size for the complete trace would be 128×128, at which ε is set to 0.15.

The value of W, which depends on the incompleteness and noise, reflects the difficulty of reconstructing a FROG trace. By considering different values of W and adopting the most suitable iterative parameters, the algorithm can be made more efficient. Considering two special cases of noise: firstly, in the absence of noise, the first term becomes 1, and $W = \eta$, indicating

Optics EXPRESS

that the reconstruction difficulty only depends on the incompleteness. Secondly, when the noise approaches infinity, $W = 0$, indicating an extremely high level of reconstruction difficulty. Table 1 shows the parallel iteration parameters of the MPPA for traces with varying W, detailing the number of sub-traces, iteration times and update coefficients. During the parallel reconstruction processes, only a few rapid iterations on sub-traces are needed to identify results close to the correct pulse. Then interpolations serve as the initial guesses for the subsequent grids. And a maximum of 200 iterations (external loops) are allowed in the global trace. In the process of updating the new pulse guess, the update coefficients α varies according to a uniform random distribution within the internal loop to enhance the convergence [32]. Here we employ different uniform distribution ranges for the update coefficients corresponding to traces of varying sizes: $U(0.8,1)$, $U(0.4,0.6)$, $U(0.1,0.3)$ for traces of increasing size, respectively.

Table 1. Parameters used for the MPPA method. Number of sub-traces and iterations, and update parameters per sub-trace with W from 0 to 1

	$I_{M/4\times N/4}$			$I_{M/2\times N/2}$			$I_{M\times N}$	
Weight factor, W	K_2	#of iterations	α	K_1	#of iterations	α	K_0	α
≧0.5	16	5	$U(0.8,1)$	8	5	$U(0.4,0.6)$	4	$U(0.1,0.3)$
[0.2,0.5)	20	10		10	5		4	
[0.1,0.2)	24	10		12	10		4	
[0.04,0.1)	32	20		16	10		8	
<0.04	48	20		24	20		8	

The consideration of the W factor further enhances the stable convergence effect of the multi-grid parallel iteration process across various traces. This is achieved by leveraging the fact that each sub-trace's iterations are independent and executed in parallel on multiple processor cores.

3. Results

3.1. MPPA reconstruction of incomplete traces

Next, we demonstrate the performance of the MPPA in retrieving pulses from incomplete traces, and juxtapose it with the commonly used the ptychographic-based reconstruction algorithm. To this end, we numerically generate a series of random pulses. The process commences with a random complex array in the time domain, which is subsequently multiplied by Gaussian intensity envelopes successively in both the time and frequency domains [11]. The ideal *TBP* is obtained by adjusting the width of both the temporal and spectral Gaussian intensities. First, we generate 1000 random initial pulses with $TBP = 5$, and the grid size of the noiseless simulated FROG traces is 128×128. The G error is adopted to represent the accuracy of reconstruction results, which is expressed as

$$G = \sqrt{\frac{1}{MN}\sum_{i=1}^{N}\sum_{j=1}^{M}|I_{ret}(\omega_i,\tau_j) - \mu I_{orig}(\omega_i,\tau_j)|^2}, \tag{10}$$

where μ is a real normalization constant that minimizes G error, and I_{ret} and I_{orig} represent the normalized retrieved and the original FROG traces, respectively. It is commonly accepted that, when the signal occupies a significant portion of the trace, the G error is less than 1%, signifying convergence.

To investigate the pulse retrieval capability of MPPA in instances of incomplete traces, we focus on two prevalent cases in practical applications: spectrally filtered traces and temporally

Optics EXPRESS

under-sampled traces. The former can be attributed to the limited matching bandwidth of the nonlinear crystal or the spectrometer [31]; the latter can reduce the number of scanning delays, greatly shorten the sampling time, and effectively mitigate the impact of time window limitations and time jitter [33]. Next, we applied both the MPPA and ptychographic-based algorithm (random update parameters were used) to retrieval these 1000 unknown pulses in both cases, subsequently calculating the reconstructed G errors for each pulse. All original traces were sized at 128×128 pixels. We have selected the best stopping criteria in the iterations, i.e., the maximum G error or G' error (G' is normalized by the trace area, rather than the number of points) [34]. To illustrate the convergent stability of the algorithms for different pulse retrievals, all algorithms were run only once for all pulses. It should be noted that while the final error is typically expressed as either G or G', these two types of error patterns are consistent when the trace size is appropriately chosen. Herein, we present only the results of G errors.

Figures 2(a)-(c) show an example of these two cases. Figure 2(a) presents a complete, noiseless trace. Figures 2(b) and (c) present the spectrally filtered trace and the temporally under-sampled traces with $\eta = 0.1$, respectively. Figures 2(d) and (e) present a comparison of G errors for varying values of η using the MPPA and ptychographic-based algorithm, respectively. Figure 2(d) shows the comparison for spectrally filtered traces and Fig. 2(e) shows the comparison for temporally under-sampled traces. The mean values and standard deviations (error bars) have been computed for both converged and non-converged G errors. The results show that when $\eta \geq 0.1$, the outcomes of both spectrally filtered traces and temporally under-sampled traces are almost convergent, with small fluctuation across different pulses. However, the ptychographic-based algorithm performs much less well. It is important to note that although the ptychographic-based algorithms achieve over 80% convergence when $\eta \geq 0.5$, a small number of non-converging pulses result in significant average errors. Specifically, when $\eta = 0.1$, the maximum error is $G = 0.009$ or $G' = 0.12$, and the convergence rates for the MPPA in both two cases exceed 99%, while those for the ptychographic-based algorithm are both only about 5%. Clearly, the MPPA significantly improves the correct convergence for incomplete traces and avoids false local minima.

3.2. MPPA reconstruction from noisy traces

Noise is a significant factor that cannot be overlooked. Therefore, we also investigated the performance of the MPPA in pulse retrieval under varying noise conditions and compared it with the results obtained from the ptychographic-based algorithm. In the presence of strong noise, the G error cannot accurately reflect the reconstruction error. Therefore, in numerical simulations of the noise impact, we evaluate the error of reconstruction using error angle, which is defined as [13]

$$\delta(E, \hat{E}) = \arccos\left(\frac{\left|\left\langle \widehat{E}(t)|E(t)\right\rangle\right|}{\sqrt{\left\langle \widehat{E}(t)|\widehat{E}(t)\right\rangle \langle E(t)|E(t)\rangle}}\right), \tag{11}$$

where $\widehat{E}(t)$ and $E(t)$ are the original and reconstructed pulsed electric fields, respectively, and $\langle f(t)|g(t)\rangle = \int f(t)\overline{g(t)}dt$ stands for the inner product. δ effectively represents the consistency of the retrieved time-domain pulse field. When assessing the quality of reconstruction in SHG FROG, several well-known trivial ambiguities arise: trivial time shifts, temporal direction and absolute phase. To remove the temporal ambiguity in retrieved pulses in numerical simulations, certain treatments must be applied to both the original and retrieved pulses: the maximum intensity of the original pulse is set to a delay 0, and the phase is initialized with center at 0. Then the cross-correlations between the original pulse and both the retrieved pulse and its time-flipped conjugate pulse (its temporally ambiguous pulse) are calculated. The reconstructed pulse is then determined as the result of the minimum cross-correlation pulse.

Optics EXPRESS

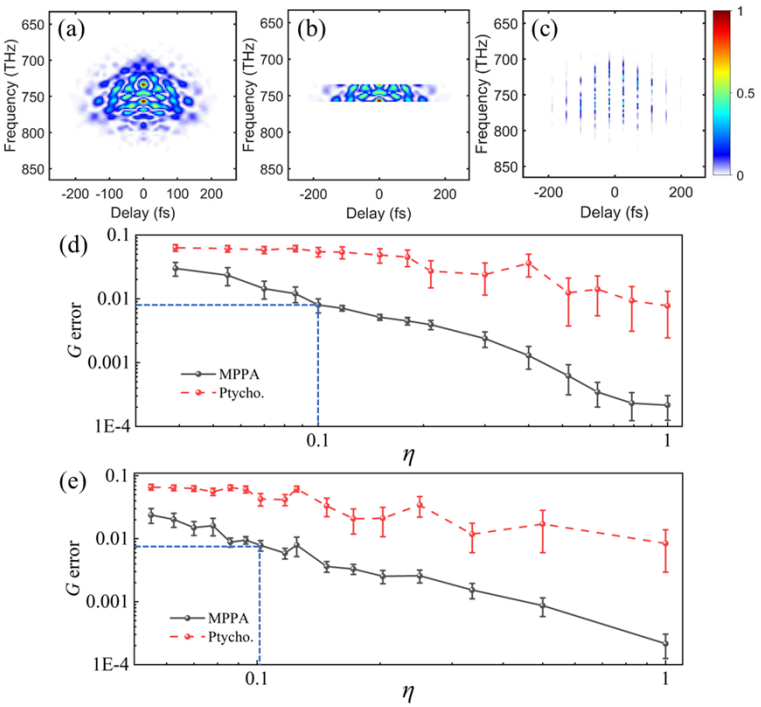

Fig. 2. Pulse reconstructions from FROG traces that were spectrally filtered and temporally under-sampled using the MPPA and ptychographic-based reconstruction algorithm, respectively. (a) An exemplary original complete noiseless trace. (b) The spectrally filtered trace. (c) The temporally under-sampled trace. (d) The variation curves of the G errors of spectrally filtered traces using the MPPA and ptychographic-based algorithm. (e) The variation curves of the G errors of temporally under-sampled trace using the MPPA and ptychographic-based algorithm. The averages and standard deviations (error bars) of the G errors over 1000 pulses are calculated, both for converged and non-converged results.

Figure 3 shows the convergence performance for complete traces and two cases of incomplete traces with noise. We investigate the error angles of the MPPA and ptychographic-based algorithm under varying noise levels and incompleteness η, again choosing the above 1000 pulses and Gaussian white noise was added to all traces [35]. Figure 3(a) shows the comparative results for complete traces ($\eta = 1$). Figure 3(b) shows the comparative results of the two algorithms with $\eta = 0.1$ and $\eta = 0.3$ for spectrally filtered traces, and Fig. 3(c) shows the comparative results of the two algorithms with $\eta = 0.1$ and $\eta = 0.33$ for temporally under-sampled traces. Larger average degree errors and standard deviations were observed in the ptychographic-based algorithm during pulse retrieval for incomplete traces with significant noise. In contrast, the reconstruction stability of the MPPA is excellent, with the degree errors of all pulses essentially consistent. For $\eta = 0.1$ FROG traces in the presence of strong noise of 10 dB, the convergence rate of the MPPA for spectrally filtered traces is 92%, while that of the ptychographic-based algorithm is only 7%, and for temporally under-sampled traces, the convergence rate of the MPPA is 90%, while that of the ptychographic-based algorithm is only 5%. The results indicate that, even in the presence of 10 dB noise, the MPPA can still retrieve pulses from highly incomplete traces ($\eta = 0.1$) and is noticeably superior to the ptychographic-based algorithm.

Figure 4 presents an example of pulse reconstruction using the MPPA under this extreme condition ($\eta = 0.1$ and $SNR = 10$ dB). Figures 4(a)–(b) show the complete and noisy trace, respectively. Figures 4(c)–(f) display the reconstruction results from the spectrally filtered trace,

Optics EXPRESS

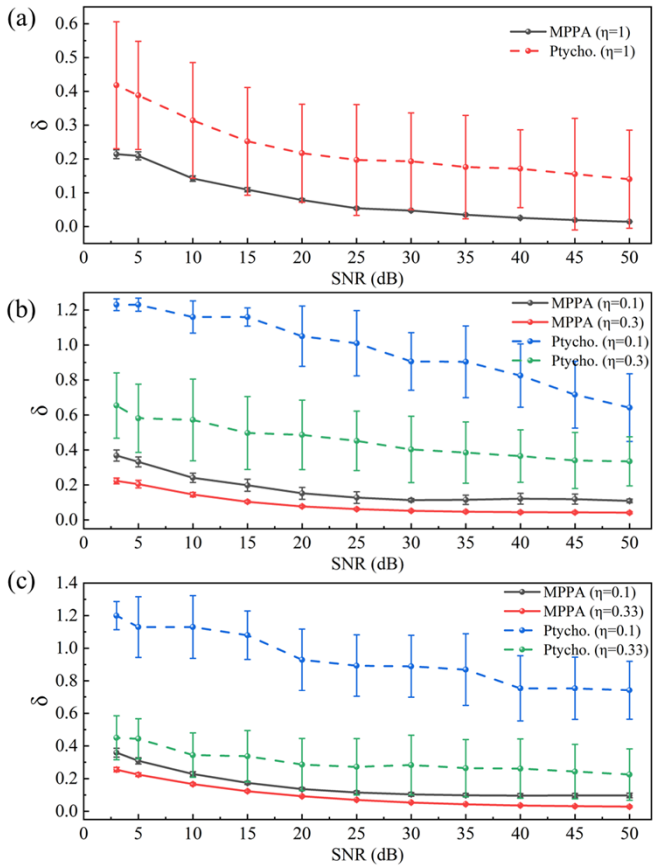

Fig. 3. Error angles of the MPPA and ptychographic-based algorithm under different noise levels and incompleteness η for 1000 random pulses. (a) The comparison results for complete traces ($\eta = 1$). (b) The comparison results with $\eta = 0.1$ and $\eta = 0.3$ for spectrally filtered traces. (c) The comparison results with $\eta = 0.1$ and $\eta = 0.33$ for temporally under-sampled traces. The averages and standard deviations (error bars) of the G errors over 1000 pulses are calculated, both for converged and non-converged results.

which include the incomplete trace, the reconstructed trace, the reconstructed time-domain pulse field, and the frequency-domain pulse field, respectively. The error angle $\delta = 0.184$. Figures 4(g)–(j) are the corresponding reconstruction results obtained from the temporally under-sampled trace. The error angle $\delta = 0.178$. Despite significant noise interference, the reconstructed pulse still largely aligns with the original pulse, with the exception of the noise base present at the edges. For those traces, although the final error angle slightly exceeds the commonly accepted allowable value ($\delta = 0.1$), it still fluctuates within a very small range and exhibits stable convergence. Clearly, high-quality reconstructions can be achieved using the MPPA even when the FROG traces are significantly filtered and contaminated by noise.

3.3. *MPPA reconstruction for extremely complex pulses*

In instances where the pulse is exceedingly complex (TBP > 40), such as supercontinuum, a complete trace necessitates a minimum size of 1024×1024 or even 4096×4096. This requirement renders both the measurement and reconstruction of the trace notably cumbersome. Consequently, it becomes imperative to minimize the number of delays in practice, as this can

Optics EXPRESS

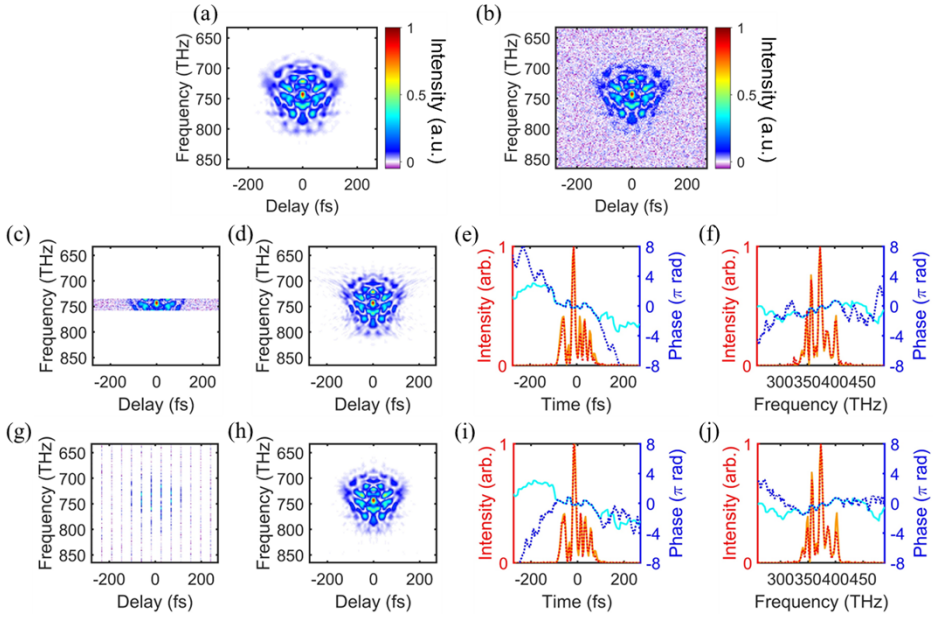

Fig. 4. Results of the MPPA for 10 dB noise and incomplete FROG traces. (a)-(b) are the simulated and the 10 dB noise FROG traces; (c)-(f) are the reconstructed results of the spectrally filtered trace, which are the incomplete trace, the reconstructed trace, reconstructed time-domain pulse field, and frequency-domain pulse field, respectively. (g)-(j) are the corresponding reconstruction results of temporally under-sampled trace. The original intensity and phase are shown in red solid curves and blue solid curves, respectively, and the retrieved intensity and phase are shown as dashed curves.

markedly diminish the duration required for data acquisition and processing. In this context, we demonstrate superior performance of the MPPA when the delay is significantly reduced.

In our numerical simulation, we generated a complex pulse with a complete trace size of 2048×2048 and *TBP* of about 80. The iteration parameters were established in accordance with Table 1, while the scaling constant ε was set to 1. For all iterations, the maximum error in judging convergence is a G error = 0.005 or G' error = 0.07. Figure 5 shows the reconstruction results of this pulse utilizing a mere 48 delays. The grid size of the trace is 2048×48, with an incompleteness η of only 0.0234. Figure 5(a) represents the original temporally under-sampled FROG trace. Figure 5(b) illustrates the FROG trace with 20 dB noise. Figure 5(c) represents the reconstructed FROG trace achieved through the MPPA, and Fig. 5(d) represents the difference between the reconstructed and the original FROG traces. Figure 5(e) is the retrieved time-domain intensity and phase of the pulse with $\delta = 0.0955$.

Compared to the ptychographic-based algorithm, the MPPA significantly enhances the retrieval of extremely complex pulses, even with a limited number of delays. For a 2048×48 trace, our results for running 100 times are almost convergent (>95%) and the reconstructed pulses closely align with the original pulse. However, none reconstruction of the ptychographic-based algorithms achieved convergence within a maximum of 200 iterations. Further increasing the maximum number of iterations to 1000 results in a slight improvement in convergence, achieving approximately 10% convergence, but this significantly increases the runtime cost. The uncertainty associated with such unreliable convergence significantly reduces the efficiency of the ptychographic-based algorithm. Overall, for complex pulses with large-size traces, the MPPA converges much more rapidly and stably than does the ptychographic-based algorithm. This

Optics EXPRESS

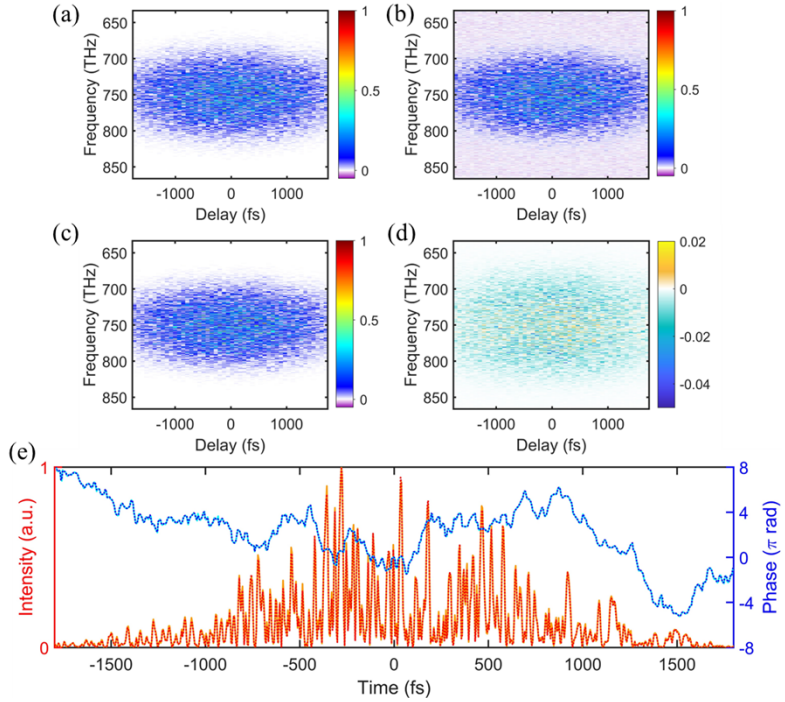

Fig. 5. Results of the MPPA for an extremely complex temporally under-sampled FROG trace with 20 dB noise. (a)-(b) are the simulated original and the 20 dB noise FROG traces; (c) is the reconstructed FROG trace using the MPPA; (d) is the difference between the reconstructed and the original traces; (e) is the result of the reconstructed time-domain pulse field. The original temporal intensity and corresponding phase are shown in red solid curve and blue solid curve, respectively, and the retrieved temporal intensity and phase are shown as dashed curves.

highly stable convergence property provides the MPPA with a significant advantage, enabling it to achieve pulse retrieval with very few (1/40) delays or spectra.

4. Pulse reconstruction of experimental data

We experimentally demonstrate the reliability of the MPPA algorithm, utilizing a homemade SHG FROG. The laser pulses were produced by a femtosecond ultrafast amplifier (Spectra-Physics Solstice Ace), characterized by a central wavelength of 800 nm, a repetition rate of 1kHz. The maximum output pulse energy is 7mJ. The measurement results are shown in Fig. 6, where Fig. 6(a) represents the measured noisy trace with a delay step of 6.67fs. The grid size of the measured FROG trace is 128×128. The pulse was reconstructed from the complete FROG trace using the ptychographic-based algorithm and the MPPA, respectively, with only a de-baseline noise treatment applied to the measured trace prior to processing. The reconstruction results are shown in Figs. 6(b) and 6(c), respectively. The G errors between the measured and reconstructed traces are 0.0063 and 0.0058, respectively. Figure 6(d) shows the reconstructed intensities and phases of the pulse. Figure 6(e) shows the reconstructed spectra and spectral phases. The results of the ptychographic-based algorithm are represented by solid curves, while the results of the MPPA are represented by dashed curves. For the reconstruction of complete traces, both ptychographic-based algorithm and MPPA exhibit small G errors in their converged cases.

Optics EXPRESS

Notably, the MPPA was able to attain an almost perfect convergence rate of nearly 100%, while the ptychographic-based algorithm attains a convergence rate of approximately 90%. The experimental result clearly indicates the presence of significant uncompensated dispersion, especially the third-order dispersion, which instigates oscillations on the temporal waveform and markedly diminishes the pulse contrast (note that SHG-FROG is not able to resolve the temporal direction).

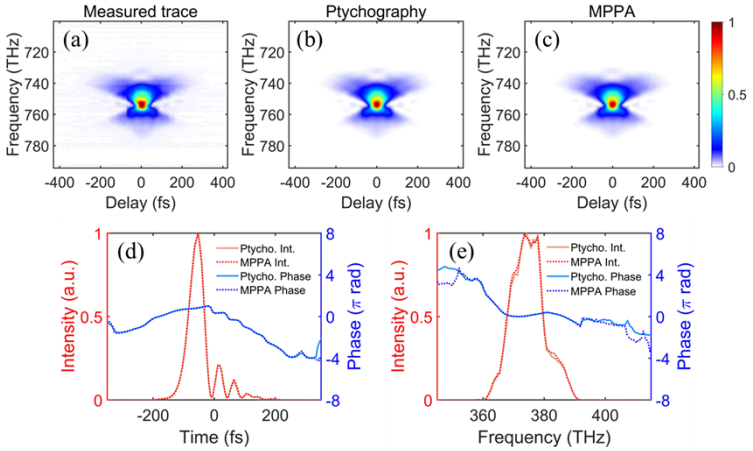

Fig. 6. Experimental pulse reconstructions from complete FROG traces. (a) Measured FROG trace. (b) and (c) are the traces reconstructed by ptychographic-based algorithm and MPPA, respectively. (d) reconstructed intensity (in red) and phase (in blue) of the pulse by the ptychographic-based algorithm (solid curve) and the MPPA (dashed curve), respectively. (e) reconstructed spectrum (in red) and spectral phase (in blue) by the ptychographic algorithm (solid curve) and the MPPA (dashed curve), respectively.

Next, we provide experimental evidence that the MPPA is capable of retrieving pulses from incomplete FROG traces while maintaining exceptionally stable convergence and accuracy. We examine the extreme case of incompleteness, with a value of approximately 0.1. We conducted independent applications of the ptychographic-based algorithm and the MPPA, each for 100 times, to the reconstruction of these incomplete traces. Figure 7(a) presents the results when the incompleteness of the spectrally filtered trace is approximately 0.1 (13/128). The mean G error for the MPPA is 0.0075, with a standard deviation of 0.00045, while the mean G error for the ptychographic-based algorithm is 0.0135, with a standard deviation of 0.007. Figure 7(b) presents the results when incompleteness of the temporally under-sampled trace is also approximately 0.1 (13/128). The average G error of the MPPA is 0.008, with a standard deviation of 0.00056, while the average G error of the ptychographic algorithm is 0.0117, with a standard deviation of 0.00054. Both the final G error and standard deviation of the MPPA are lower than those of the ptychographic algorithm. The convergence of the MPPA exceeds 95% ($G < 0.01$), whereas the convergence of the ptychographic algorithm does not surpass 10%. Figures 7(c)-(r) show examples of the MPPA and ptychographic reconstructions, both with corresponding mean G error. Figures 7(c)-(f) show an example of the MPPA reconstruction from the spectrally filtered trace, juxtaposed with the reconstruction of the MPPA from complete traces shown in Fig. 6. The G error is 0.0075. Figures 7(g)-(j) show the ptychographic reconstruction from this spectrally filtered trace, compared to the reconstruction from complete trace. The G error is 0. 0135. Figures 7(k)-(n) show an example of the MPPA reconstruction from the temporally under-sampled trace. The G error is 0.008. Figures 7(o)-(r) show the ptychographic reconstruction from this temporally under-sampled trace, compared to the reconstruction from

Optics EXPRESS

complete trace. The G error is 0. 0117. It can be seen that the reconstructions of the MPPA demonstrate a strong correlation, with significant deviations in the reconstructed phase primarily observed in the low-amplitude region. However, the ptychographic reconstruction results exhibit noticeable distortion, particularly evident in the reconstructed spectrum. This experimental evidence demonstrates that the MPPA is able to robustly and accurately retrieve the pulse from an incomplete FROG trace.

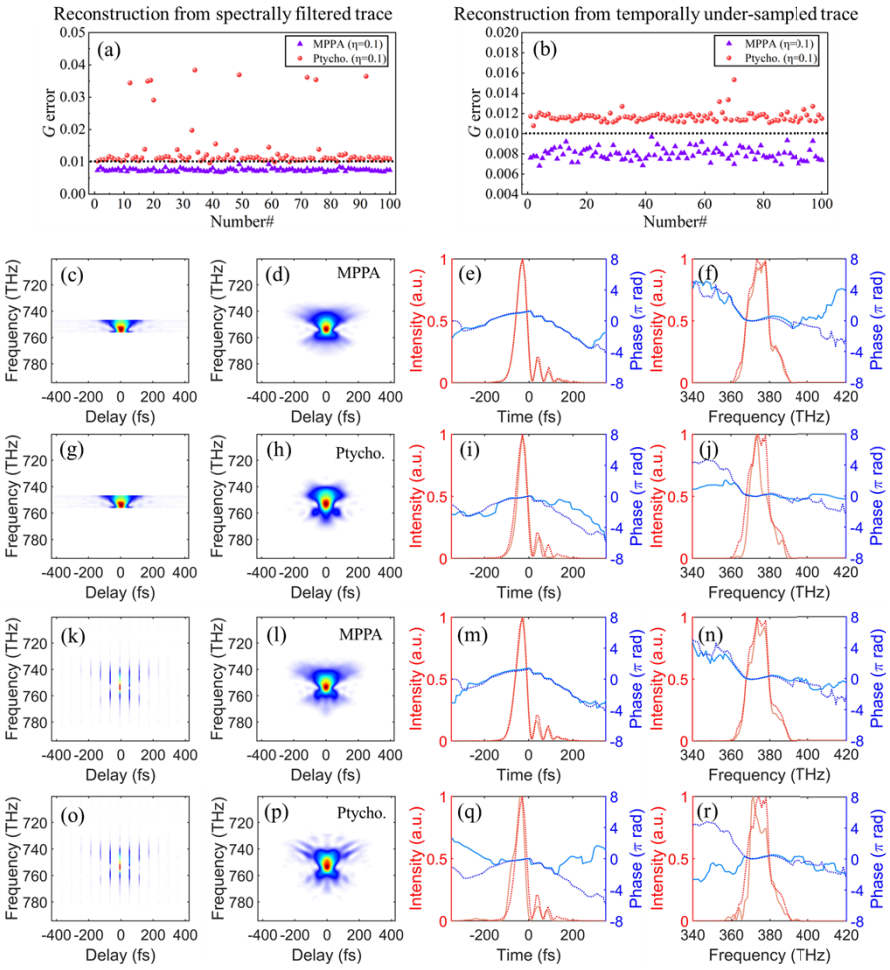

Fig. 7. Experimental pulse reconstructions from incomplete FROG traces. (a) Pulse reconstructions from experimental spectrally filtered FROG trace using the MPPA and ptychographic-based algorithm. (b) Pulse reconstructions from experimental temporally under-sampled FROG trace using the MPPA and ptychographic-based algorithm. (c)-(f) An example of the MPPA reconstruction (solid curves) from the spectrally filtered trace, compared to the reconstruction from complete traces (dash curves). (g)-(j) the ptychographic reconstruction (solid curves) from the spectrally filtered trace, compared to the reconstruction from complete traces (dash curves). (k)-(n) An example of the MPPA reconstruction (solid curves) from the temporally under-sampled trace, compared to the reconstruction from complete traces (dash curves). (o)-(r) the ptychographic reconstruction (solid curves) from the temporally under-sampled trace, compared to the reconstruction from complete traces (dash curves). All partial and reconstructed traces are presented with the same color map as in Fig. 6(c).

Optics EXPRESS

5. Discussion

The MPPA, which is based on the multi-grid parallel ePIE processes, exhibits excellent performance, particularly in the reconstruction of noisy and incomplete FROG traces. The primary advantages of the MPPA are twofold. Firstly, due to the multi-grid sampling, parallel processing of the trace and the progressive screening, the algorithm is less likely to stall at local minima. Thus, we anticipate its enhanced effectiveness in cases such as incomplete traces with high noise, significantly mitigating the pulse retrieval burden for large *TBP*. Secondly, the MPPA capitalizes on the rapid convergence characteristic of ptychography, eliminating the necessity for delay and frequency axes to adhere to Fourier relations. Although the convergence rate of the ptychographic-based algorithm remains high (over 90%) for complete traces without prior information, it markedly diminishes for notably noisy and incomplete traces. The MPPA utilizes almost all the information from the trace by flexible sampling and determines parallel iteration parameters by weighting factors, thereby mitigating the erroneous convergence during parallel iterations on different sub-traces.

While ensuring a significant enhancement in convergence, the convergence speed of the MPPA is also exceedingly rapid. The algorithm based on ptychography is a type of algorithm with very fast convergence speed, compared, for example, to PCGPA. The MPPA is based on parallel ePIE iterations and, in the case of accurate convergence, it converges faster for complex pulses than the ptychographic-based algorithm. For example, for the pulses with $TBP = 5$ and $N = 128$, the average convergence time of the ptychographic-based algorithm is 0.134s, while the MPPA has an average convergence time of 0.212s due to additional overhead in sampling and parallel computation. For the pulses with $TBP = 100$ and $N = 4096$, however, the average convergence time of the ptychographic-based algorithm is 105s, while the MPPA converges more rapidly at 69s. In contrast, the convergence time of PCGPA is 0.30s and 31 min in these two cases, respectively [11]. Importantly, when reconstructing a pulse from an incomplete trace, the convergence of the MPPA is significantly improved, and its advantage in reconstruction speed is also greater.

The MPPA can achieve 100% convergence on complete traces, and significantly improve the convergence of incomplete traces, typically achieving about 90% convergence at $\eta = 0.1$ and $SNR = 10$ dB. While the MPPA utilized part (the multigrid component) of the RANA approach, complete implementation of the RANA approach would also provide a better initial guess, obtained from the frequency marginal of SHG trace based on Paley-Wiener Theorem, before iterations (interpolation would be required for an incomplete trace), thereby further enhancing the convergence by the complete combination of the MPPA and RANA.

Drawing from both numerical and experimental results, we believe that the MPPA holds significant importance for FROG measurements, particularly when reconstructing single-shot, unstable, and complex pulses. It should be noted that the convergence enhancement effect of the MPPA is particularly evident for complex pulses. This can be attributed to the fact that the FROG trace greatly estimates the pulse. The swift fluctuations in intensity within the immediate vicinity of complex pulse traces offer a more comprehensive information, thereby adequately characterizing the pulse. In contrast, simpler pulses, such as those with Gaussian waveforms or spectra, necessitate a larger area for the convergence of their traces. However, the data acquisition and processing of these simpler pulses are straightforward. The MPPA plays a pivotal role in ensuring the stable convergence of FROG pulse measurements. Subsequently, we will delve into more intricate scenarios. For instance, the stability of the MPPA guarantees the measurement of pulse instability [36].

Finally, The MPPA demonstrates significant applicability, as it can be easily implemented in all versions of FROG by modifying the expression of $G(t)$ during the iteration process, such as PG, transient grating (TG), self-diffraction (SD). Furthermore, when the power spectrum of the gate pulse is provided, a double-blind detection can be realized, thereby enabling simultaneous retrieval of two pulses in both cross-FROG (XFROG) and FROG-CRAB.

Optics EXPRESS

6. Conclusion

In summary, we implement what we call the multi-grid parallel ptychographic algorithm for pulse retrieval, which enables rapid screening of pulses during the iteration by leveraging multi-grid parallel ePIE iterative processes, thereby avoiding local minima until convergence to the global trace is achieved. We have both numerically and experimentally demonstrated that the MPPA exhibits excellent pulse retrieval performance, characterized by good robustness and stable convergence, particularly for incomplete and noisy FROG traces. Despite the presence of 10 dB noise, this method can accurately converge to the correct pulse using merely 1/10 of the measured delays or spectra. For extremely complex pulses with very high *TBPs*, complete pulse retrieval can be accomplished with even less than 1/40 delays. Overall, the MPPA offers a stable and reliable reconstruction method for diverse complex or incomplete traces, significantly broadening the measurement range of individual measuring devices, obviating numerous tedious tasks, and opening up many new opportunities for the diagnosis of ultrashort laser pulses.

Funding. Chinese Academy of Sciences (XDA25020105, XDA25020306, 181231KYSB20170022, CXJJ-21S015); National Natural Science Foundation of China (12004403, 12074399, 12204500, 62175247); Ministry of Science and Technology of the People's Republic of China (2021YFE0116700); Science and Technology Commission of Shanghai Municipality (24ZR1474900, 19560713700, 22YF1455300, 20ZR1464400).

Disclosures. Rick Trebino owns and Rana Jafari occasionally consults for Swamp Optics, a company that sells FROG devices. The other authors declare no potential conflicts of interest.

Data availability. Data underlying the results presented in this paper are not publicly available at this time but may be obtained from the authors upon reasonable request.

References

1. C. Iaconis and I. A. Walmsley, "Spectral phase interferometry for direct electric-field reconstruction of ultrashort optical pulses," Opt. Lett. **23**(10), 792–794 (1998).
2. Y. Cai, Z. Chen, S. Zheng, *et al.*, "Accurate reconstruction of electric field of ultrashort laser pulse with complete two-step phase-shifting," High Power Laser Sci. Eng. **7**, e13 (2019).
3. A. Trisorio, S. Grabielle, M. Divall, *et al.*, "Self-referenced spectral interferometry for ultrashort infrared pulse characterization," Opt. Lett. **37**(14), 2892–2894 (2012).
4. M. Miranda, C. L. Arnold, T. Fordell, *et al.*, "Characterization of broadband few-cycle laser pulses with the d-scan technique," Opt. Express **20**(17), 18732–18743 (2012).
5. I. Sytcevich, C. Guo, S. Mikaelsson, *et al.*, "Characterizing ultrashort laser pulses with second harmonic dispersion scans," J. Opt. Soc. Am. B **38**(5), 1546–1555 (2021).
6. R. Trebino, R. Jafari, S. A. Akturk, *et al.*, "Highly reliable measurement of ultrashort laser pulses," J. Appl. Phys. **128**(17), 171103 (2020).
7. R. Trebino, *Frequency-resolved optical gating: the measurement of ultrashort laser pulses* (2002).
8. R. Trebino, K. W. DeLong, D. N. Fittinghoff, *et al.*, "Measuring ultrashort laser pulses in the time-frequency domain using frequency-resolved optical gating," Rev. Sci. Instrum. **68**(9), 3277–3295 (1997).
9. T. Bendory, P. Sidorenko, and Y. C. Eldar, "On the Uniqueness of FROG Methods," IEEE Signal Process. Lett. **24**(5), 722–726 (2017).
10. K. W. DeLong, D. N. Fittinghoff, R. Trebino, *et al.*, "Pulse retrieval in frequency-resolved optical gating based on the method of generalized projections," Opt. Lett. **19**(24), 2152–2154 (1994).
11. R. Jafari, T. Jones, and R. Trebino, "100% reliable algorithm for second-harmonic-generation frequency-resolved optical gating," Opt. Express **27**(3), 2112–2124 (2019).
12. R. Jafari and R. Trebino, "Extremely Robust Pulse Retrieval From Even Noisy Second-Harmonic-Generation Frequency-Resolved Optical Gating Traces," IEEE J. Quantum Electron. **56**(1), 1–8 (2020).
13. P. Sidorenko, O. Lahav, Z. Avnat, *et al.*, "Ptychographic reconstruction algorithm for frequency-resolved optical gating: super-resolution and supreme robustness," Optica **3**(12), 1320–1330 (2016).
14. P. Sidorenko, O. Lahav, Z. Avnat, *et al.*, "Ptychographic reconstruction algorithm for frequency resolved optical gating: super-resolution and extreme robustness: erratum," Optica **4**(11), 1388–1389 (2017).
15. J. M. Rodenburg and H. M. L. Faulkner, "A phase retrieval algorithm for shifting illumination," Appl. Phys. Lett. **85**(20), 4795–4797 (2004).
16. A. M. Maiden and J. M. Rodenburg, "An improved ptychographical phase retrieval algorithm for diffractive imaging," Ultramicroscopy **109**(10), 1256–1262 (2009).
17. T. Witting, D. Greening, D. Walke, *et al.*, "Time-domain ptychography of over-octave-spanning laser pulses in the single-cycle regime," Opt. Lett. **41**(18), 4218–4221 (2016).
18. A. M. Heidt, D. M. Spangenberg, M. Brugmann, *et al.*, "Improved retrieval of complex supercontinuum pulses from XFROG traces using a ptychographic algorithm," Opt. Lett. **41**(21), 4903–4906 (2016).

Optics EXPRESS

19. M. Murari, G. D. Lucarelli, M. Lucchini, *et al.*, "Robustness of the ePIE algorithm for the complete characterization of femtosecond, extreme ultra-violet pulses," Opt. Express **28**(7), 10210–10224 (2020).
20. M. Lucchini, G. D. Lucarelli, M. Murari, *et al.*, "Few-femtosecond extreme-ultraviolet pulses fully reconstructed by a ptychographic technique," Opt. Express **26**(6), 6771–6784 (2018).
21. M. Lucchini, M. H. Brügmann, A. Ludwig, *et al.*, "Ptychographic reconstruction of attosecond pulses," Opt. Express **23**(23), 29502–29513 (2015).
22. A. J. Mao and C. P. Liu, "Reconstruction of an ultrashort laser pulse from flexibly shaped FROG traces via ptychography algorithm," Laser Phys. **30**(12), 125301–125306 (2020).
23. J. R. Fienup and C. C. Wackerman, "Phase-retrieval stagnation problems and solutions," J. Opt. Soc. Am. A **3**(11), 1897–1907 (1986).
24. S. Pinilla, J. Bacca, and H. Arguello, "Phase retrieval algorithm via nonconvex minimization using a smoothing function," IEEE Trans. Signal Process. **66**(17), 4574–4584 (2018).
25. S. Pinilla, T. Bendory, Y. C. Eldar, *et al.*, "Frequency-resolved optical gating recovery via smoothing gradient," IEEE Trans. Signal Process. **67**(23), 6121–6132 (2019).
26. D. J. Kane and A. B. Vakhtin, "A review of ptychographic techniques for ultrashort pulse measurement," Prog. Quantum Electron. **81**, 100364 (2022).
27. T. Bendory, D. Edidin, and Y. C. Eldar, "On signal reconstruction from FROG measurements," Applied and Computational Harmonic Analysis **48**(3), 1030–1044 (2020).
28. R. Jafari and R. Trebino, "High-speed "multi-grid" pulse-retrieval algorithm for frequency-resolved optical gating," Opt. Express **26**(3), 2643–2649 (2018).
29. Y. S. G. Nashed, D. J. Vine, T. Peterka, *et al.*, "Parallel ptychographic reconstruction," Opt. Express **22**(26), 32082–32097 (2014).
30. H. Lin, W. Xu, and F. Zhang, "Parallel data acquisition and reconstruction method of near-field ptychography for large samples," Opt. Express **29**(26), 43342–43352 (2021).
31. K. W. DeLong, D. N. Fittinghoff, and R. Trebino, "Practical issues in ultrashort-laser-pulse measurement using frequency-resolved optical gating," IEEE J. Quantum Electron. **32**(7), 1253–1264 (1996).
32. M. Köhl, A. A. Minkevich, and T. Baumbach, "Improved success rate and stability for phase retrieval by including randomized overrelaxation in the hybrid input output algorithm," Opt. Express **20**(15), 17093–17106 (2012).
33. P. Veselá and K. Žídek, "Influence of the delay line jitter on the SHG FROG reconstruction," Opt. Express **29**(3), 4392–4404 (2021).
34. R. P. Scott, N. K. Fontaine, J. Cao, *et al.*, "High-fidelity line-by-line optical waveform generation and complete characterization using FROG," Opt. Express **15**(16), 9977–9988 (2007).
35. D. N. Fittinghoff, K. W. DeLong, R. Trebino, *et al.*, "Noise sensitivity in frequency-resolved optical-gating measurements of ultrashort pulses," J. Opt. Soc. Am. B **12**(10), 1955–1967 (1995).
36. M. Rhodes, G. Steinmeyer, J. Ratner, *et al.*, "Pulse-shape instabilities and their measurement," Laser Photonics Rev. **7**(4), 557–565 (2013).